A MAGNETO-ELASTIC SENSOR FOR MEASURING PRESSURE OSCILLATIONS IN COMMON RAIL SYSTEMS

Julian Baumann * **Dirk Göger** * **Uwe Kiencke** *

* *Institute of Industrial Information Technology, University of Karlsruhe (TH)*

Abstract: The trend in developing common rail injection systems goes to higher injection pressures and smaller minimum injected fuel masses. Multiple injection patterns generate pressure oscillations on the connection pipe between common rail and injector. These oscillations influence the amount and progression of the injected fuel mass and therefore the combustion process. As the oscillations depend on many different parameters, it is impossible to calculate their exact progression analytically.
In this paper a new, non-invasive pressure sensor for measuring the pressure at the injector is introduced. It is based on the magneto-elastic effect and does not involve any mechanical elements. The physics on which the sensor is based are explained and the sensor design as well as a signal processing algorithm to reconstruct the pressure are illustrated. Measurement results are presented as well.

Keywords: Automotive control, Diesel engines, fuel injection, magnetic properties, pressure measurement

1. INTRODUCTION

The steadily increasing market share of Diesel engines with common rail injection systems indicates the success of this relatively young technology. The main advantage of the common rail system is the decoupling of pressure generation and the injection process which offers various kinds of injection patterns, as the latest generation of injectors features several pre, main, and post injections during one injection cycle.

Engine developers work on reducing fuel consumption, noise, and emissions by optimizing the combustion process. This is achieved by increasing on the one hand the preciseness of the injection process and on the other hand the homogeneity of the air-fuel mixture inside the cylinder. Therefore the injection pressure continuously rises for each new generation of injection systems while the smallest possible injected fuel mass decreases concurrently.

Due to multiple injection patterns the injector needle opens and closes in short time intervals, which excites pressure oscillations on the connection pipe between injector and common rail. Typical pressure oscillations measured with a highly accurate reference sensor are shown in Figure 1. These pressure oscillations are depending on the injection pattern, the injector characteristics, the hydraulic properties of the connection pipe, the rail pressure, and the fuel viscosity and temperature. Due to the high amount of influencing parameters it is an unsolved problem to analytically compute the time response of the pressure at the injector with sufficient accuracy. But as the exact pressure progression at the injector is of

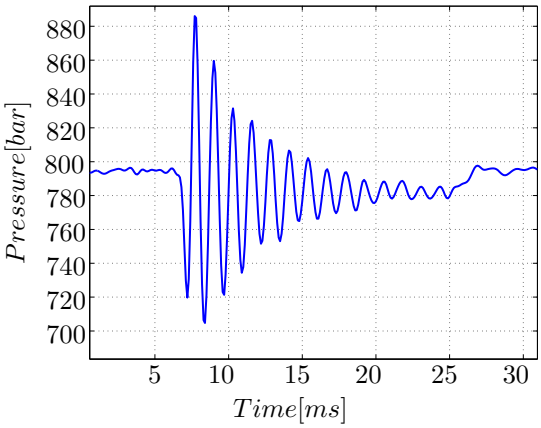

Fig. 1. Typical pressure oscillations in common rail systems

importance for the accuracy of the injected fuel mass and therefore for the combustion process, its knowledge could significantly improve the efficiency and reduce the emissions of the engine.

To solve this problem, the *Institute of Industrial Information Technology* is developing a new pressure sensor based on the *magneto-elastic effect*, called ME-sensor. Conventional pressure sensors that work in a high dynamic range are often based on the piezo-resistive effect and are unaffordable for mass use in automobiles. The advantage of the ME-sensor over these conventional sensors is its low cost design and that it is working non-invasively. The disadvantage is a lower signal to noise ratio and its sensitivity to disturbances.

The paper is structured as follows. After a short introduction to the basic magnetic principles and the magneto-elastic effect the design of the sensor is presented. The measured signals are processed through a signal processing algorithm to extract the pressure on the connection pipe. This algorithm is implemented in real time on a fixed point processor. Results of the pressure reconstruction are presented.

2. MAGNETO-ELASTIC EFFECT

Atoms of ferromagnetic materials have a magnetic dipole moment which is aligned parallel in certain areas, the so-called domains. The magneto-elastic effect, which is the physical background on which the sensor introduced in this paper is based, depends on the behavior of these domains (Cullity, 1972). To explain the magneto-elastic effect, the better known reverse effect of magnetostriction will be discussed first.

2.1 Magnetostriction

Magnetostriction can be seen as the magnetic counterpart of the piezo-electric effect. An external magnetic field $\boldsymbol{H}$ will change the dimensions of a ferromagnetic workpiece. Figure 2 shows the principle of the effect.

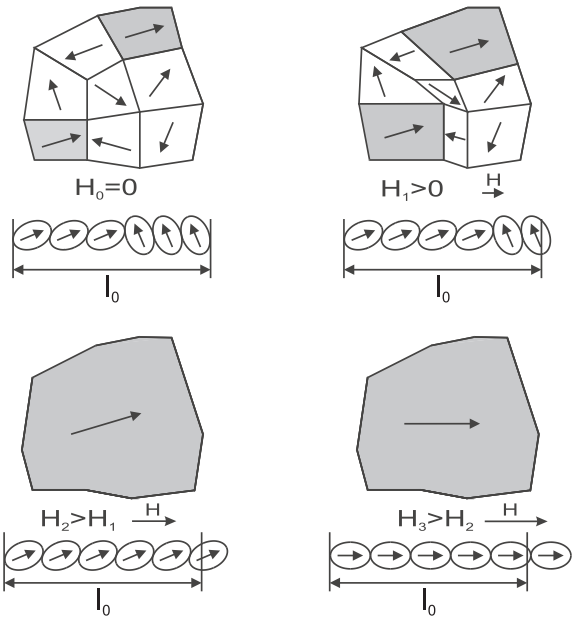

Fig. 2. Magnetic constriction as a domain process

In an unmagnetized material the direction of the magnetic moments are distributed statistically so that the resulting overall-moment is zero and the workpiece has the length l_0, see upper left part of Figure 2. When applying an external magnetic field $\boldsymbol{H}$ the domains that have approximately the same direction as the external field grow at the expense of the other domains. Due to the ellipsoid course of the electrons this process is accompanied by an increasing workpiece length in field direction, see upper right part of Figure 2. With increasing field force more domains get the same orientation as the external field (lower left part of Figure 2). Finally all domains have the same orientation and the saturation expanse is reached, see lower right part of Figure 2. This process is called magnetostriction and is characterized by the material constant

$$\lambda_s = \frac{\Delta l}{l} \quad . \tag{1}$$

Depending on the material λ_s is positive or negative. The reverse effect is called magneto-elastic effect (ME-effect).

2.2 ME-Effect

The magneto-elastic effect is also known as *Villari effect* (Villari, 1865). It describes the change of the domain orientation of a material under mechanical stress. According to the sign of the magneto-constriction constant λ_s of the material, a mechanical tension σ effects an increase or decrease of the magnetization directed towards tension. This means that the hysteresis curve of the

material which describes the nonlinear connection between magnetic flux density $\boldsymbol{B}$ and magnetic field $\boldsymbol{H}$ is warped. As an example Figure 3 shows the qualitative hysteresis curve of Nickel (Ni) for a workpiece under different tension σ.

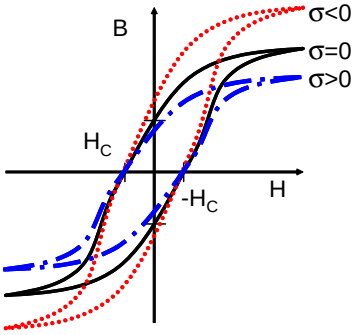

Fig. 3. Warped hysteresis curve of Nickel due to ME-effect

The working point dependent parameter is the magnetic permeability μ_r that describes the ratio of magnetic flux density and magnetic field

$$\boldsymbol{B} = \mu_0 \mu_r \boldsymbol{H} \quad . \tag{2}$$

A medium flowing under pressure through a metal tube will produce radial and tangential tension with different signs in the tube wall, see Figure 4.

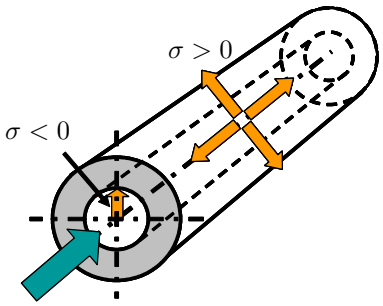

Medium $\longrightarrow$ Pressure p

Fig. 4. Tangential and radial stress in a tube

A changing pressure $\dot{p}$ causes a change of mechanical stress $\dot{\sigma}$ in the wall of the tube. The magneto-elastic effect generates a change of the magnetic permeability $\dot{\mu_r}$ which leads to a time-varying magnetic flux density $\dot{\boldsymbol{B}}$. According to Faraday's law this will induce a voltage in a coil mounted on the tube which can be measured as the sensor output signal. This coherence can be written as

$$\dot{p} \rightarrow \dot{\sigma} \overset{ME-Effect}{\longrightarrow} \dot{\mu_r} \rightarrow \dot{B} \rightarrow U_{ind} \quad . \tag{3}$$

Up to now it is not possible to calculate the exact induced voltage U_{ind} analytically out of the pressure change $\dot{p}$ inside the tube. A detailed explanation of the correlating atomic incidents of the magneto-elastic effect can be found in (Lee, 1955), but because of many unknown material properties and parameters no useful model could be generated.

3. SENSOR THEORY AND DESIGN

To measure the induced voltage according to (3), the sensor was designed as a cylindric coil. As the signal of interest is the pressure close to the injector, this coil was winded around the connection pipe from the rail to the injector. Additionally, two pre-magnetization coils were added next to the measurement coil. The sensor structure is shown in Figure 5.

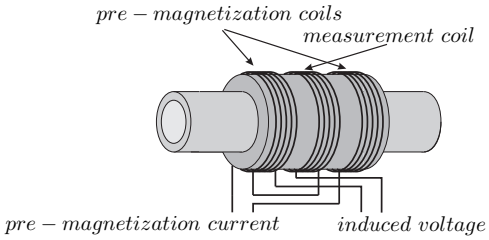

Fig. 5. Structure of the ME-sensor

The pre-magnetization coils are used to adjust the working point of the sensor. A DC current is applied which generates an external magnetic field $\boldsymbol{H}$. For a long cylindric coil the magnetic field can be approximated by

$$\boldsymbol{H} = \frac{N_1 \cdot I}{l} \quad , \tag{4}$$

where N_1 is the number of windings, l is the axial length of the coil and I is the current. The magnetic permeability μ_r and therefore the magnetic flux density $\boldsymbol{B}$ nonlinearly depend on the $\boldsymbol{H}$-field, see Figure 3. Therefore the pre-magnetization coils can be used to specify in which area of the hysteresis curve the sensor is operated.

Under the assumption of a constant cross-sectional area A of the coil Faraday's law can be written as

$$\begin{aligned} U_{ind} &= -N_2 \cdot \dot{\phi} \\ &= -N_2 \left(\int \boldsymbol{B} \, dA \right)^{\cdot} \\ &= -N_2 \cdot \dot{\boldsymbol{B}} \cdot A \quad , \end{aligned} \tag{5}$$

where ϕ is the magnetic flux and N_2 is the number of windings of the measurement coil. $\dot{\boldsymbol{B}}$ can be expressed with (2) and with a constant $\boldsymbol{H}$-field the only time-varying variable due to the pressure oscillations is μ_r

$$U_{ind} = -N_2 \cdot \mu_0 \, \dot{\mu_r} \, \boldsymbol{H} \cdot A \quad . \tag{6}$$

Substituting $\boldsymbol{H}$ with (4) results in

$$U_{ind} = -N_1 \cdot N_2 \cdot A \cdot \mu_0 \, \dot{\mu_r} \, \frac{I}{l} \quad . \tag{7}$$

This equation is valid with one limitation. The magnetic field inside the coil core is smaller than the one outside. The reason for this is that the magnetic circuit is closed over the air-gap when the coil core (which is the connection pipe) is

a rod instead of a toroid. The air-gap generates a demagnetizing field $\boldsymbol{H_N}$ inside the rod which points in opposite direction to the external field. Therefore, the resulting field $\boldsymbol{H_i}$ inside the coil core is much smaller than the external field $\boldsymbol{H_e}$ calculated by (4). Figure 6 schematically shows the different fields outside and inside the rod.

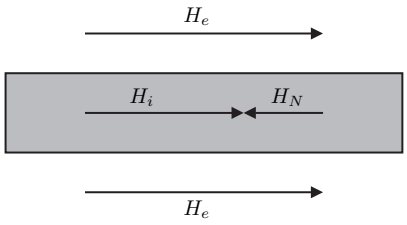

Fig. 6. Demagnetizing field inside the rod

With help of the magnetization $\boldsymbol{M}$ follows

$$\boldsymbol{H_i} = \boldsymbol{H_e} - \boldsymbol{H_N} = \boldsymbol{H_e} - N \cdot \boldsymbol{M} \quad , \qquad (8)$$

where N is the shape-depending demagnetization factor ranging between 0 and 1. A toroidal core has a demagnetization factor $N = 0$, a finite rod one of $N = 0.01$ (Boll, 1990). Therefore a much higher external magnetic field $\boldsymbol{H_e}$ is necessary to generate the same flux density $\boldsymbol{B}$ in a rod core than in a toroidal core.

(3) and (7) indicate that U_{ind} is proportional to the derivative of the magnetic permeability $\dot{\mu}_r$ and that this derivative is linearly depending on the pressure derivative $\dot{p}$. The second of these statements is surely only an approximation of the complex atomic coherences in the material. Nevertheless it is a good basis for reconstructing the pressure from the induced voltage, as will be explained in the next chapter.

4. SIGNAL PROCESSING

For testing purposes the sensor was mounted on a connection pipe between injector and rail on a common rail injection test bench at the Institute of Industrial Information Technology. The test bench is equipped with four state-of-the-art common rail injectors and a pump which can generate up to $2000bar$ pressure. The injectors are controlled by an ECU [1] which allows flexible injection patterns with pre, main and post injection.

Other sensor layouts like the use of a yoke have been tested before (Torkzadeh *et al.*, 2002). As the measurement results were not more promising, the sensor with the cheapest layout, which is the cylinder sensor shown in Figure 5, was employed for further investigation.

Figure 7 shows the voltage induced in the measurement coil during an injection of $500\mu s$ opening

[1] Engine Control Unit

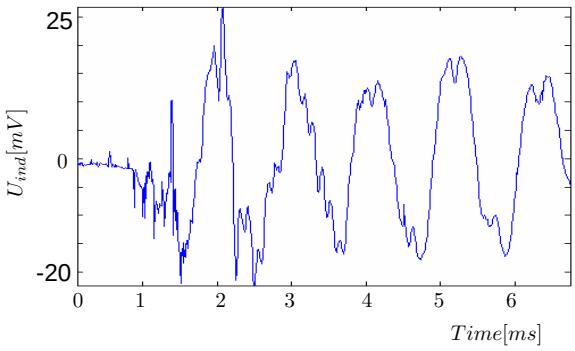

Fig. 7. Induced voltage during pressure oscillations

time at $800bar$ rail pressure, which is the same working point as in Figure 1. The induced voltage qualitatively shows the same characteristics as the reference signal but disturbances have significant influence. The aim was to create a signal processing algorithm that eliminates disturbances in the induced voltage and reconstructs the pressure progression as measured by the reference sensor. Therefore, correlated measurements with ME-sensor and a reference sensor mounted next to it on the same tube were carried out and the two signals were compared.

4.1 Filtering and Integration

To better understand which part of the ME-signal origins from a disturbance and which part indicates the pressure variations, the fourier transform of both ME-signal and reference signal was calculated, see Figure 8. The spectrum of the reference sensor (Figure 8(b)) shows a high frequency content around $f = 800Hz$. It also has a component at $f = 0Hz$ because the reference sensor outputs the absolute pressure. The frequency content of the ME-sensor (Figure 8(a)) also shows a high peak around $f = 800Hz$. Additionally, there are peaks at $f = 50Hz$ and $f = 150Hz$ which can be clearly identified as disturbances and some frequency components at $f = 2.7kHz$ which are lacking in the reference sensor spectrum.

Based on these observations a high pass filter for eliminating the low-frequency disturbances of the ME-signal and a low pass filter for eliminating the frequency content above $1.6kHz$ were designed.

As the aim is to get the absolute pressure in the tube but the ME-effect only delivers a signal proportional to the pressure derivative $\dot{p}$, (3) is integrated and delivers

$$p = p_0 + k \cdot \int U_{ind,filtered}\, dt \quad , \qquad (9)$$

where k is a scaling factor and p_0 the pressure at the beginning of the integration. To avoid drifting of the integrated signal, the integration is only

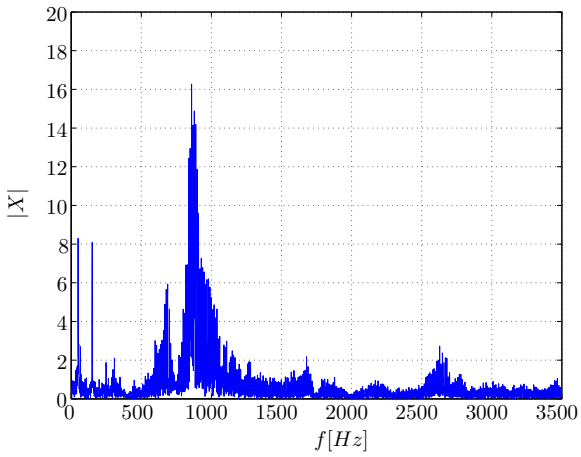

(a) Spectrum of the ME-sensor signal

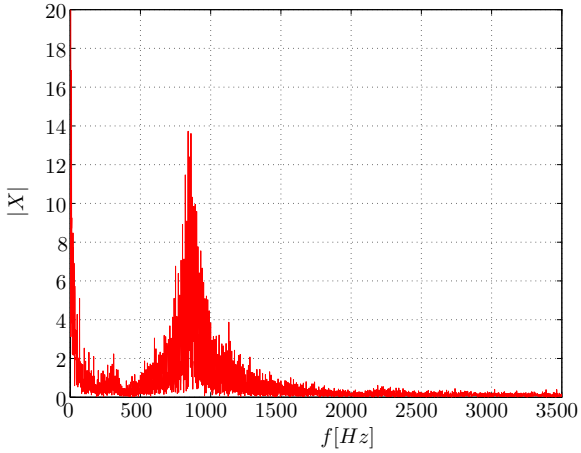

(b) Spectrum of the reference sensor signal

Fig. 8. Frequency content of the signals during a pressure oscillation

carried out for a certain time period after an injection. The pressure p_0 is the working point and can be derived from the standard rail pressure sensor, so the equation for pressure reconstruction is

$$p_{rec} = p_{rail} + k \cdot \int U_{ind,filtered}\, dt \quad . \qquad (10)$$

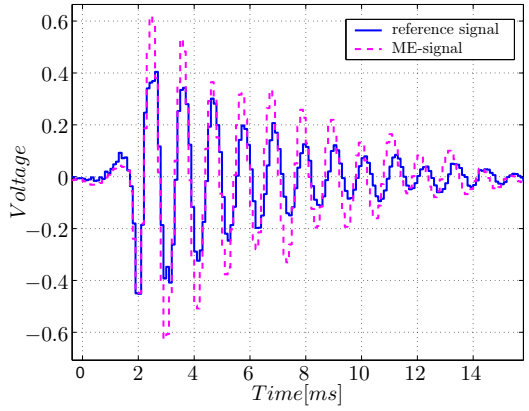

Fig. 9. Filtered and integrated ME-signal compared with reference signal

As the rail damps the oscillations and the rail pressure sensor cannot acquire high frequency components, it only outputs the mean rail pressure p_{rail} without oscillations. A comparison of the reconstructed signal p_{rec} according to (10) with the reference signal is shown in Figure 9. At the beginning of the pressure oscillations the reconstructed signal matches with the reference signal very well. Afterwards, the damping of the oscillations in the reference signal is higher.

4.2 Time-Varying Damping Factor

In order to match the two signals in Figure 9 as close as possible the envelopes of the two signals are compared. The ratio of the two envelopes shows an exponentially damped course which can be approximated by a third order polynomial. The ME-signal is then multiplied by this course which acts as a time-varying damping factor k^*. The trigger point for the start of k^* is derived from the injector current which indicates the start of an injection.

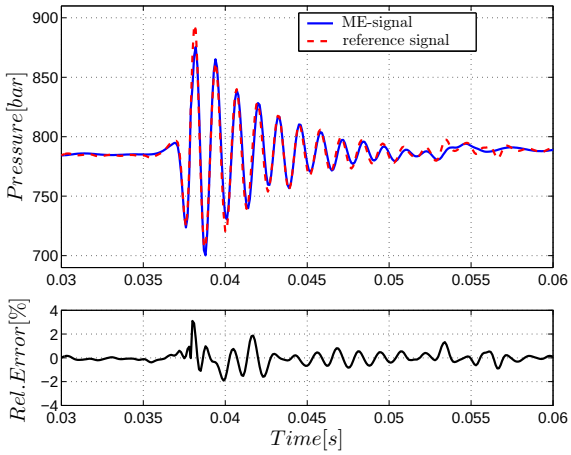

Fig. 10. ME-signal scaled with time-varying damping factor k^* compared with reference signal and relative error

The scaled ME-signal is shown in Figure 10. The relativ error

$$F_r = \frac{p_{ref} - p_{rec}}{p_{ref}} \qquad (11)$$

is always smaller than 4% and in most areas even smaller than 2%. This also holds for the statistical variation of other injections at the same working point. The pressure reconstruction algorithm therefore is sufficiently exact.

4.3 Implementation on Fixed Point Processor

The algorithm introduced in section 4.1 and 4.2 was implemented on a dual processor hardware consisting of an Infineon C167 micro controller

and a Motorola XC56309 $100MHz$ DSP which both operate with fixed point arithmetics. The induced voltage was amplified and then acquired by an ADC. The filtering, integration, and scaling was carried out on the DSP. The filters were realized as IIR filters to reduce the computational effort compared with FIR filters. High attention was paid to reduce the influence of quantization effects by appropriate scaling of the signals and to avoid limit cycles as the poles of the filters lie close to the unit circle. The micro controller was responsible for communicating the results of the DSP to a RS232 interface. Moreover, a CAN interface was implemented to send key values of the reconstructed pressure to an ECU. It was possible to run the complete algorithm in real time at $50kHz$ sampling frequency.

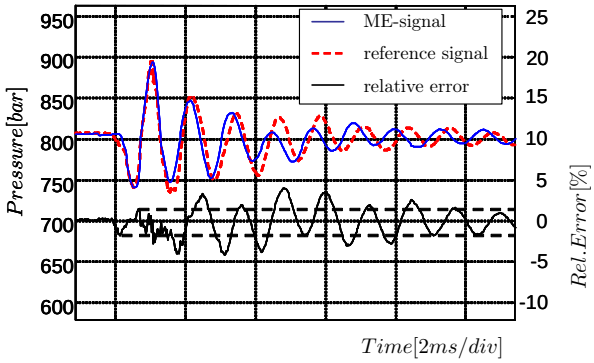

Fig. 11. Results of pressure reconstruction on fixed point processor

The results of the computation can be seen in Figure 11. In the beginning the reconstructed signal matches the reference signal very well. With decreasing amplitude of the oscillations the error increases due to a phase shift in the ME-signal. This may arise from the non-constant group delay of the IIR filters. A lower sampling frequency might enable the use of the computational more expensive FIR filters which have the advantage of a constant group delay and therefore avoid phase distortions.

5. CONCLUSION

As the last paragraphs showed, the magnetoelastic effect can be used to measure the pressure deviations in an injection tube. The introduced signal processing algorithm reconstructed the pressure signal with sufficient accuracy at an working point of $800bar$ rail pressure and $500\mu s$ injector opening time. Other relevant working points between 200 and $1500bar$ showed similar results. One drawback is that the time-varying scaling function up to now changes with the rail pressure.

The sensor design, consisting of three coils of wire winded around the tube, is inexpensive. The sensor works non-invasive and is therefore easy to mount. Problems like density of the mounting and changing the hydraulic properties of the injection system, as they are known for conventional high pressure sensors, do not arise. The sensor needs a signal processing unit which might be realized as an ASIC in serial production. Some of the filters can also be implemented in analogue hardware. The sensor can be rated as a low prized application to access up to now unknown information about the pressure close to the injector. It may also be used to monitor the functionality of the injection system.

The sensor has to be tested for robustness in the area of an operating engine, where magnetic and electric fields might disturb the induced voltage. The influence of pipes from different batches, which of course will be a key point in industrial application, has to be studied thoroughly.

ACKNOWLEDGEMENTS

This project is a co-operation between Siemens VDO Automotive AG, Regensburg, Germany, and the Institute of Industrial Information Technology, University of Karlsruhe (TH), Germany. We especially like to thank Jürgen Fritsch and Thomas Schlegl from Siemens VDO for their dedicated support of this project.

CONTACT

The authors can be reached through the Institute of Industrial Information Technology, University of Karlsruhe (TH), Germany at +49(721)608-4518, or baumann@iiit.uni-karlsruhe.de.

REFERENCES

Boll, Richard (1990). *Weichmagnetische Werkstoffe*. Vacuumschmelze GmbH, Hanau.

Cullity, B. D. (1972). *Introduction to Magnetic Materials*. Addison-Wesley.

Lee, Eric W. (1955). Magnetostriction and magnetomechanical effects. *Reports on progress in physics* **18**, 184–229.

Torkzadeh, Dara D., Uwe Kiencke and Martin Keppler (2002). Introduction of a new non-invasive pressure sensor for common-rail systems. In: *SAE Technical Paper 2002-01-0842*. Detroit.

Villari, E. (1865). Ueber die Aenderungen des magnetischen Moments, welche der Zug und das Hindurchleiten eines galvanischen Stroms in einem Stabe von Stahl oder Eisen hervorbringt. *Ann. Phys. Chem.* **126**, 87–122.